Available online at www.sciencedirect.com

ScienceDirect

Geochimica et Cosmochimica Acta 264 (2019) 105–117

Geochimica et Cosmochimica Acta

www.elsevier.com/locate/gca

Evidence for subsolidus quartz-coesite transformation in impact ejecta from the Australasian tektite strewn field

Fabrizio Campanale [a,b,*], Enrico Mugnaioli [b], Luigi Folco [a], Mauro Gemmi [b], Martin R. Lee [c], Luke Daly [c,e,f], Billy P. Glass [d]

[a] Dipartimento di Scienze della Terra, Università di Pisa, V. S. Maria 53, 56126 Pisa, Italy
[b] Center for Nanotechnology Innovation@NEST, Istituto Italiano di Tecnologia (IIT), Piazza San Silvestro 12, 56127 Pisa, Italy
[c] Department of Geographical and Earth Sciences, University of Glasgow, Glasgow G12 8QQ, UK
[d] Department of Geosciences, University of Delaware, Newark, DE, USA
[e] Australian Centre for Microscopy and Microanalysis, University of Sydney, Sydney 2006, NSW, Australia
[f] Space Science and Technology Centre, School of Earth and Planetary Science, Curtin University, Bentley, 6102 WA, Australia

Received 1 April 2019; accepted in revised form 11 August 2019; Available online 21 August 2019

Abstract

Coesite, a high-pressure silica polymorph, is a diagnostic indicator of impact cratering in quartz-bearing target rocks. The formation mechanism of coesite during hypervelocity impacts has been debated since its discovery in impact rocks in the 1960s. Electron diffraction analysis coupled with scanning electron microscopy and Raman spectroscopy of shocked silica grains from the Australasian tektite/microtektite strewn field reveals fine-grained intergrowths of coesite plus quartz bearing planar deformation features (PDFs). Quartz and euhedral microcrystalline coesite are in direct contact, showing a recurrent pseudo iso-orientation, with the [1 $\bar{1}$ 1]* vector of quartz near parallel to the [0 1 0]* vector of coesite. Moreover, discontinuous planar features in coesite domains are in textural continuity with PDFs in adjacent quartz relicts. These observations indicate that quartz transforms to coesite after PDF formation and through a solid-state martensitic-like process involving a relative structural shift of $\{1\ 0\ \bar{1}\ 1\}$ quartz planes, which would eventually turn into coesite (0 1 0) planes. This process further explains the structural relation observed between the characteristic (0 1 0) twinning and disorder of impact-formed coesite, and the $\left\{1\ 0\ \bar{1}\ 1\right\}$ PDF family in quartz. If this mechanism is the main way in which coesite forms in impacts, a re-evaluation of peak shock pressure estimates in quartz-bearing target rocks is required because coesite has been previously considered to form by rapid crystallization from silica melt or diaplectic glass during shock unloading at 30–60 GPa.

Keywords: Impact ejecta; Australasian tektite strewn field; Shock metamorphism; Subsolidus quartz-to-coesite transformation; Martensitic mechanism

1. INTRODUCTION

Quartz is one of the most common minerals in Earth's continental crust. Under shock metamorphism it displays a wide range of effects including mechanical twins, planar fractures (PFs), planar deformation features (PDFs), diaplectic glass (densified glass), and lechatelierite (silica glass). The study of shock metamorphism of quartz, and high-pressure silica polymorphs, i.e. coesite and stishovite, is therefore relevant to defining the physical conditions attained during the majority of hypervelocity impacts of

* Corresponding author at: Dipartimento di Scienze della Terra, Università di Pisa, V. S. Maria 53, 56126 Pisa, Italy.
E-mail address: fabrizio.campanale@phd.unipi.it (F. Campanale).

https://doi.org/10.1016/j.gca.2019.08.014
0016-7037/

cometary or asteroidal bodies on Earth, as well as quartz-rich surfaces elsewhere in the Solar System.

Coesite is rare at the Earth's surface but can occur in exhumed deep-seated metamorphic rocks such as kimberlites (e.g., Smyth and Hatton, 1977). On the other hand, coesite is a fairly common product of impact cratering and indeed it is one of the most important and reliable indicators of shock events. Coesite was synthetized for the first time by Coes (1953) and later discovered in nature by Chao et al. (1960) in sheared Coconino sandstone deposits at the 1.2 km diameter Barringer Crater (Arizona). This mineral has been the subject of numerous studies seeking to understand how silica polymorphs react under sudden and extreme P-T gradients. These studies include computational simulations (e.g., Luo et al., 2003; Bourova et al., 2004; Merli and Sciascia, 2013), shock recovery experiments (e.g., Wackerle, 1962; Grady et al., 1975; Stöffler and Langenhorst, 1994), and the analysis of impact rocks from craters ranging in size from the 45 m diameter Kamil crater in Egypt (Fazio et al., 2014; Folco et al., 2018) to the 24 km diameter Ries crater in Germany (e.g., Shoemaker and Chao, 1961; Stöffler, 1971; Fazio et al., 2017) and the 300 km diameter Vredefort structure in South Africa (e.g., Martini, 1978, 1991; Spray and Boonsue, 2018).

In endogenic geological processes, which typically involve equilibrium reactions and timeframes ranging from years to millions of years, coesite forms from quartz at pressures between ~3 and ~10 GPa (Supplementary material Fig. S1). In impactites, coesite is preserved as a metastable phase in crystalline rocks that experienced peak shock pressures above ~30–40 GPa (e.g., Stöffler and Langenhorst, 1994), and in porous sedimentary rocks shocked at pressures as low as ~10 GPa (Kowitz et al., 2016). Moreover, coesite associated with impact events shows a characteristic pervasive disorder or polysynthetic (1 0 0) twinning, both developing along (0 1 0) composition planes (Bourret et al., 1986).

The solid-state transition of quartz to both coesite and stishovite are reconstructive transformations. This means that covalent Si—O—Si bonds between silica tetrahedra must break before the new framework can reassemble. Coesite has a pseudo-hexagonal framework that preserves silicon in tetrahedral coordination, while stishovite has a rutile-like packing with silicon in six-fold octahedral coordination. Reconstructive transformations are slow and hence it is generally believed that such subsolidus transformations do not occur either in shock experiments (with pulse durations of <1 μs) or in natural impacts even if pulse durations up to seconds are expected - depending on projectile dimensions and impact velocity (Melosh, 2012). Consequently, there is a general consensus that coesite within impactites originates by crystallisation from a dense amorphous phase during shock unloading, when the pressure release path passes through the coesite stability field (Supplementary material Fig. S1). The precursor amorphous phase may be a silica shock melt (e.g., Stöffler and Langenhorst, 1994; Fazio et al., 2017) or a highly densified diaplectic silica glass (Stähle et al., 2008).

Here we present evidence for direct solid-state quartz-to-coesite transformation in shocked coesite-bearing quartz ejecta from the Australasian tektite/microtektite strewn field, which is the largest and youngest (~0.8 Myr old) on Earth. These findings contradict current models for coesite formation yet are consistent with recent results from the Kamil crater, the smallest coesite-bearing impact crater reported so far (Folco et al., 2018). The coesite-quartz intergrowths in shocked quartz arenite from the Kamil crater suggest a quartz-to-coesite transformation that takes place during localized shock-wave reverberation at the beginning of the pore collapse process, documenting the production of localized pressure-temperature-time gradients in porous targets, as predicted by numerical models in the literature (Folco et al., 2018).

2. AUSTRALASIAN TEKTITE/MICROTEKTITE STREWN FIELD BACKGROUND

Tektites are relatively homogeneous silica-rich glass bodies formed by melting of terrestrial surface deposits during the impact of an extraterrestrial body (Taylor, 1973; Koeberl, 1994; Glass and Simonson, 2013). They are up to several tens of centimetres in size and are found scattered over large areas of the Earth's surface called strewn fields (Koeberl, 1992).

The Australasian tektite/microtektite strewn field (Fig. 1) covers ~15% of the Earth's surface, with a minimum lateral extent of 14,000 km (Glass and Simonson, 2013; Folco et al., 2016). Australasian tektites occur on land from southeast Asia over much of Australia and Tasmania. Microtektites (microscopic tektites) have also been found in the surrounding ocean basins in deep-sea sediments, and in Victoria Land, Antarctica (Folco et al., 2008).

Despite its size and young age, location of source crater for the Australasian strewn field is still debated. Many authors suggest that a >30 km diameter crater (Glass and Koeberl, 2006) should be located somewhere in Indochina to explain abundance, petrographic and geochemical trends in microtektite distribution (e.g., Glass and Koeberl, 2006; Folco et al., 2010). However, a new hypothetical location of the crater in the arid area of Northwest China, most probably in the Badain Jaran or Tengger deserts on the Alxa Plateau, has been proposed on the basis of geochemical and isotopic data (Mizera et al., 2016). Due to the lack of field evidence of a source crater, other authors have proposed that the strewn field was generated by a low-altitude airburst of an impacting comet (e.g., Wasson, 2003).

The nature of the impact target rocks that generated the Australasian strewn field is also an open question. Major and trace element analyses on tektites suggest that tektites might be the result of the mixing between at least two different rocks, such as quartz-rich sandstone and shale (e.g., Taylor, 1962; Amare and Koeberl, 2006). Taylor and Kaye (1969) suggested a sedimentary target rock, showing strong similarities in the comparison of major and trace element abundances between tektites and terrestrial sandstones, such as graywacke-subgraywacke-arkose. Mineral inclusions found in layered (or Muong Nong-type) tektites from Indochina with x-ray diffraction and

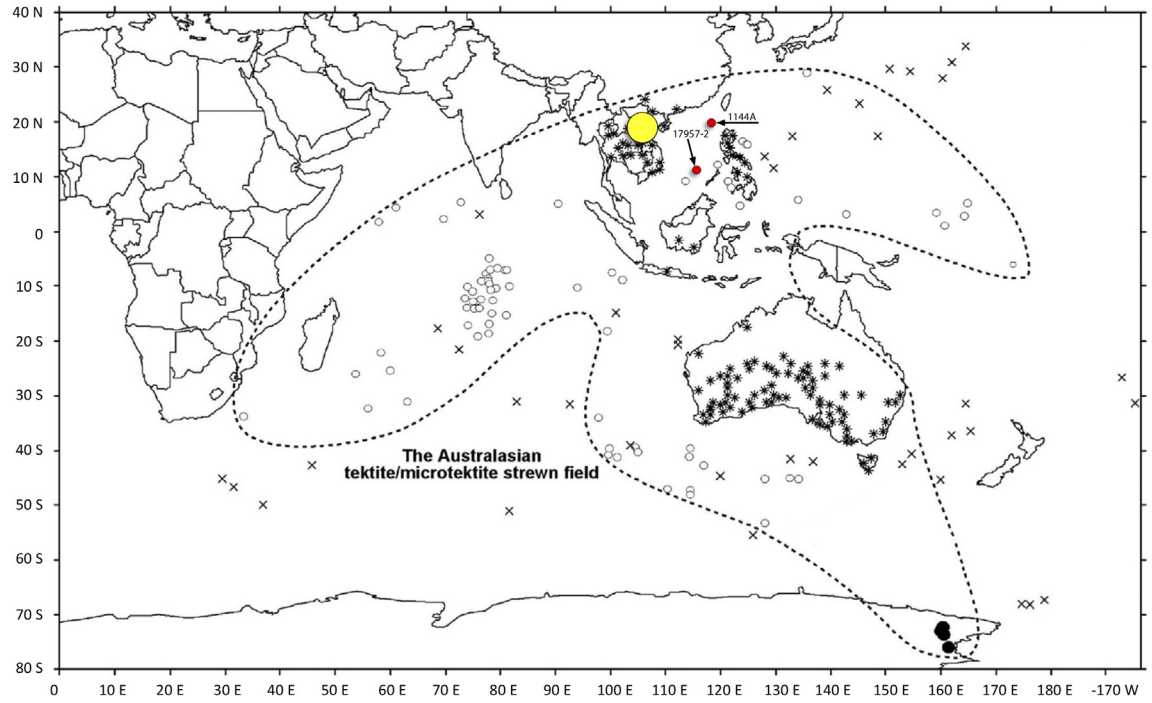

Fig. 1. The Australasian tektite-microtektite strewn field (Folco et al., 2016). Impact ejecta studied in this work (red circles) are from ODP-1144A and SO95-17957-2 cores (Glass and Koeberl, 2006; Glass and Wu, 1993). The yellow circle in Indochina represents the hypothetical source impact location. Asterisks and white circles indicate sites where tektites and microtektites were found, respectively. The ×'s represent sites in the ocean where microtektites were not found. (For interpretation of the references to colour in this figure legend, the reader is referred to the web version of this article.)

energy dispersive X-ray (EDX) analysis indicate a fine-grained sedimentary target (Glass and Barlow, 1979). More recently, Glass and Koeberl (2006) and Mizera et al. (2016), studying the ejecta found in the Australasian microtektite (AAMT) layer and Australasian tektites respectively, proposed that the parent material of the Australasian tektites/microtektites was a fine-grained, quartz-rich sedimentary deposit, possibly loess. A surface or near-surface sedimentary deposit was also suggested by ^{10}Be cosmogenic nuclide analysis (Ma et al., 2004; Rochette et al., 2018). There is thus a general consensus on a porous sedimentary parent material.

Unmelted and partly melted impact ejecta can be found together with classical glassy microtektites in the AAMT layer. These ejecta particles consist of rock fragments, which may contain coesite, rarely stishovite, and other high-pressure phases like TiO_2-II and reidite and white, opaque grains consisting of a mixture of quartz, coesite, and stishovite (Glass and Koeberl, 2006; Glass and Fries, 2008). Impact ejecta were first recognised in the >125 μm size fraction in 7 out of 33 microtektite-bearing deep-sea sediment cores obtained within 2000 km from Indochina (Glass and Wu, 1993). The discovery of these high-pressure phases provided a strong support for the impact cratering origin of tektites/microtektites and to the hypothesis that the crater is located in the Indochina area. More recently, impact ejecta in the AAMT layers were also discovered in the Ocean Drilling Program (ODP) 1143A core, in the central part of the South China Sea, and in the Sonne-95 (SO95)-17957-2 and ODP-1144A cores, from the central and northern part of the South China Sea, respectively (Glass and Koeberl, 2006).

3. SAMPLES AND METHODS

The shocked ejecta particles associated with the AAMT layer studied in this work are from two deep-sea sediment cores both located within 2000 km of Indochina (~17°N, 107°E; Fig. 1): ODP site 1144A and Sonne Core SO95-17957-2. The ejecta particles are from the >125 μm size fraction of a sediment sample from Core 37X, Section 6, 66-67 cm depth at ODP Site 1144; and from a sample from a depth of 806 cm in Core SO95-17957-2. For extraction procedures see Glass and Wu (1993). They include 569 and 141 rock fragments and mineral grains from ODP-1144A and SO95-17957-2 cores, respectively (Supplementary material Table S1).

All the particles were first characterized in terms of shape, size, color, transparency, and luster, using a ZEISS Stemi 2000 stereomicroscope (Dipartimento di Scienze della Terra, University of Pisa) equipped with an Axiocam Camera. Seventy particles ranging in size from 150 μm^2 to 500 μm^2 were selected for field emission gun - scanning electron microscopy (FEG-SEM) and Raman microspectroscopy. Twenty of these particles have (almost) pure silica composition, four of which show evidence of shock

metamorphism (i.e., PDFs and coesite) and were thus embedded in EpoFix resin, sectioned and polished for additional Raman analysis and FEG-SEM study. Five electron-transparent focused-ion beam (FIB) lamellae were cut and extracted from one ~250 μm^2 size particle (labelled '1144A_350') that has a high abundance of micro-to-nanometre scale shock features (i.e., PDFs and coesite).

Backscattered electron (BSE) images were obtained at the Centro Interdipartimentale di Scienze e Ingegneria dei Materiali (CISIM) of the University of Pisa using a FEG-SEM FEI Quanta 450 operating at 10 mm working distance, 15 kV beam acceleration and 10 nA probe current.

In order to identify quartz and coesite and for their discrimination and the subsequent selection of the best sample areas for the extraction of FIB lamelle, a preliminary Raman survey were carried out using a Jobin-Yvon Horiba XploRA Plus (University of Pisa) equipped with an Olympus BX41 microscope, a grating with 1200 grooves/mm, and Peltier-cooled charge coupled device (CCD) detector. The samples were analysed with a 532 nm solid-state laser (25 mW) using a 100× objective lens and numerical aperture 0.90. The output laser power at the sample of ~6 mW. Wavelength calibration was done utilizing the first-order phonon band of a silicon wafer at ~520 cm^{-1} (De Wolf, 1996), with a wavenumber accuracy of 0.3 cm^{-1} and spectral resolution of 1.5 cm^{-1}. The calibration was further improved using a sample of quartz (main peak at 464 cm^{-1}; Scott and Porto, 1967) before and after each session. The system was operated in the confocal mode, resulting in a spatial resolution of ~361 nm. Spectra were collected through three acquisitions with single counting times up to 120 s.

Electron-transparent lamellae were prepared for transmission electron microscopy (TEM) at the Kelvin Nanocharacterisation Centre of the University of Glasgow using a dual beam FIB FEI 200TEM FIB, following the procedure described in Lee et al. (2003). TEM and electron diffraction (ED) studies were carried out at the Center for Nanotechnology Innovation@NEST of the Istituto Italiano di Tecnologia using a ZEISS Libra operating at 120 kV and equipped with a LaB_6 source and a Bruker EDS detector XFlash6T-60. TEM images were recorded by a TRS 2 k × 2 k CCD camera. Scanning-transmission electron microscopy (STEM) images were recorded by a high-angle annular dark-field (HAADF) detector. ED data were acquired by an ASI Timepix detector (Nederlof et al., 2013), able to record the arrival of single electrons and deliver patterns that are virtually background-free.

Three dimensional (3D) ED data sets were obtained rotating the sample along the tilt axis of the TEM goniometer using the procedure described by Mugnaioli and Gemmi (2018). 3D ED acquisitions were performed in angular steps of 1° and for tilt ranges up to 90°. Due to the small size of quartz and coesite crystals and the similar contrast of these phases in STEM images, crystal position was tracked after each tilt step in TEM imaging mode. Both single-pattern and 3D ED data were acquired in nano-beam electron diffraction (NED) mode after inserting a 10 μm C2 condenser aperture, in order to have a parallel beam of about 300 nm on the sample. An extremely mild illumination was used for avoiding any alteration or amorphization of the sample. 3D ED data were reconstructed and analysed using the *ADT3D* program (Kolb et al., 2011) and specially written *Matlab* routines.

Phase/orientation maps (similar to electron backscatter diffraction; EBSD, or transmission kikuchi diffraction; TKD) were carried out using the precession-assisted crystal orientation mapping technique (PACOM; Viladot et al., 2013) which has been implemented on a Zeiss Libra TEM through a Nanomegas Digistar P1000 device. The maps were obtained by scanning an area of the sample (few square micrometres) with a nanometric beam probe, while recording the diffraction patterns in precession mode. The patterns were collected by filming the fluorescent screen of the TEM with a fast-optical CCD during the scanning procedure. A cross correlation routine, which correlates these patterns and a database of patterns generated by taking in consideration the possible phases present in the sample (coesite and quartz), allows the phase determination and the indexing of each pattern (Viladot et al., 2013). The collected maps cover areas of 4 μm^2 with a spatial resolution of 20 nm.

4. RESULTS

4.1. Scanning electron microscopy and Raman

All crystalline impact ejecta with a pure silica composition are colourless, translucent to opaque white, sometimes with yellow and red stains. Particles that show evidence of a shock metamorphic overprint are typically 150–300 μm^2 in size, as discussed below. They have a subangular to subrounded shape and are partially covered by a fine-grained micaceous matrix (Supplementary material Fig. S2), which is similar to the micaceous fraction of the 'rock fragments' reported by Glass and Koeberl (2006). These particles mostly consist of a mixture of coesite and quartz in variable proportions, the latter with multiple sets of PDFs (Fig. 2, Supplementary material Fig. S2–3). They are pristine, with no evidence of secondary processes that typically affect shock metamorphic rocks such as hydrothermal activity and post-shock thermal overprint, or even deep-sea marine alteration that they could have suffered in their sampling sites.

FEG-SEM coupled with Raman spectra suggests ejecta range from almost pure PDF-bearing quartz with traces of coesite to coesite grains with PDF-bearing quartz in variable amounts (Fig. 2). They are also associated with micrometre-sized anhedral Ti-oxides (such as rutile), and Fe-S phases (possibly pyrite), as observed on their external surface and in section. FEG-SEM analyses also revealed the first report of PDFs in the Australasian tektite strewn field, with at least three diffuse cross-cutting sets in all shocked silica particles (Figs. 2 and 3, Supplementary material Fig. S2).

The particle (1144A_350) selected for high-resolution investigation, falls within the description given above. However, it shows an impressively high abundance of shock features compared to the other particles. The PDFs are so well developed throughout the sample that they are already

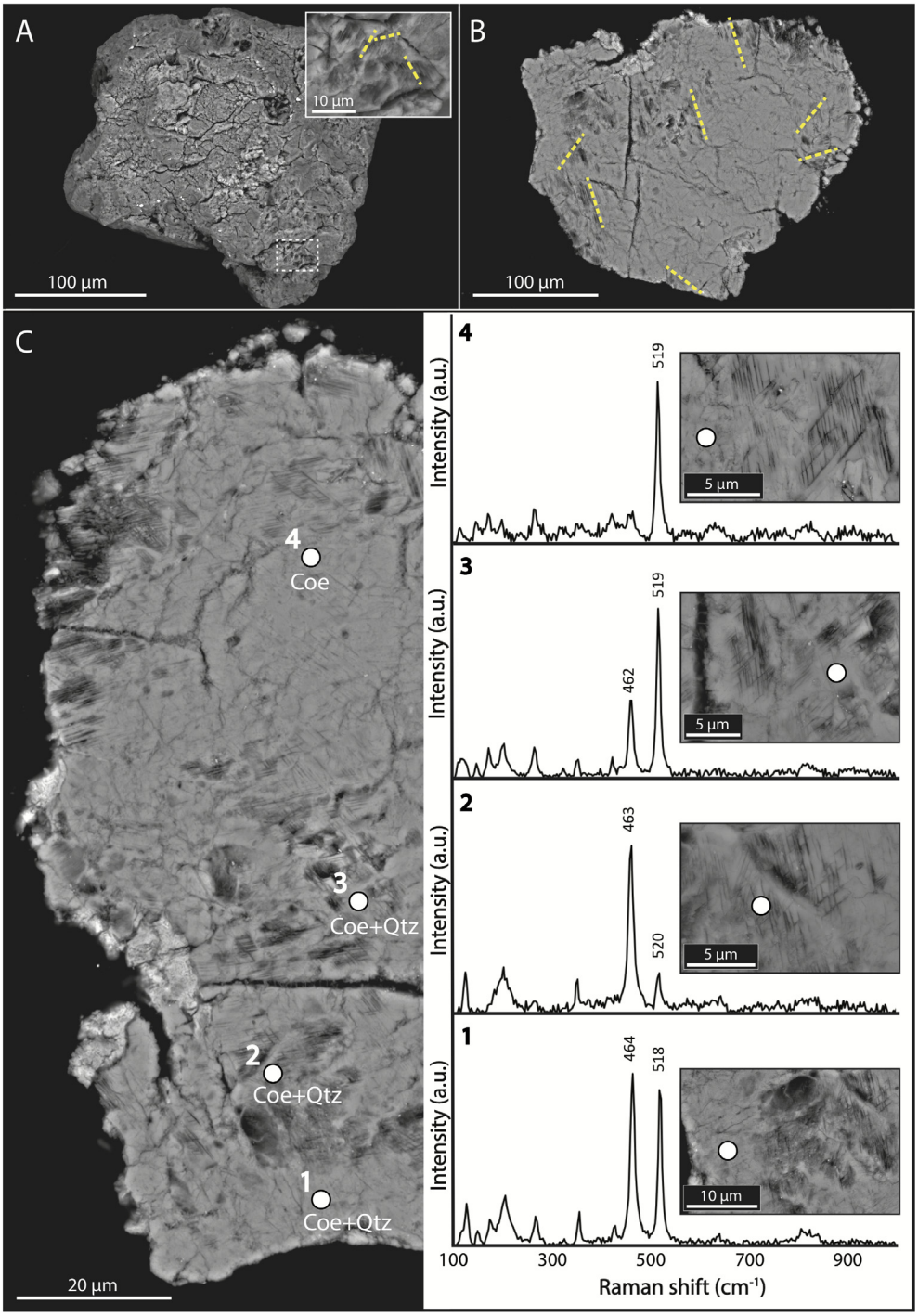

Fig. 2. BSE images and Raman data from the '1144A_350' particle. (A) The grain before polishing, showing PDFs on its external surface (see inset). (B) Sectioned particle showing PDFs throughout (highlighted with yellow dashed lines). The particle is partly surrounded by micaceous material (brighter phases at the top). (C) Enlarged image of the upper part of the sample in (B) and rotated 90° counter-clockwise, showing four Raman single spot analysis (white circles). Quartz and coesite can be recognized by their diagnostic main peaks at ~464 cm^{-1} and ~521 cm^{-1}, respectively. The mismatches of the main bands of quartz and coesite with reference values (see text) fall within the error of our system setting. (For interpretation of the references to colour in this figure legend, the reader is referred to the web version of this article.)

obvious on the external surface (Fig. 2A). Within each set, PDFs occur as parallel, narrow and closely-spaced features (average thickness: 0.5 µm; spacing from ~0.2 µm to ~0.7 µm). Raman micro-spectroscopy indicates that the portions of the particles that lack PDFs are dominated by coesite (with the spectra dominated by the coesite main peak at ~521 cm^{-1}; Liu et al., 1997), whereas the PDF-containing parts show spectra diagnostic of both coesite

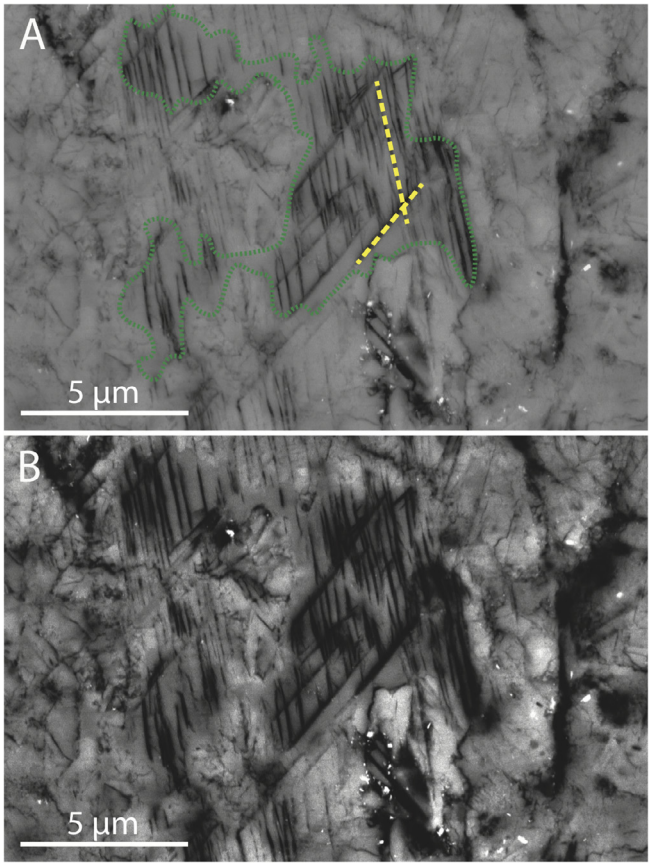

Fig. 3. BSE image of the '1144A_350' particle showing at least two sets of PDFs. (A) The contrast between quartz and coesite is appreciable through the different shades of gray of the backscatter electrons, in which coesite appears lighter than quartz. The quartz domains is highlighted by a green dotted line. PDF directions are highlighted with yellow dashed lines. The enhanced-contrast image below (B) makes the coesite more obvious, showing microcrystalline coesite grains between the sets of PDFs. (For interpretation of the references to colour in this figure legend, the reader is referred to the web version of this article.)

and quartz (~464 cm^{-1}; Scott and Porto, 1967) – with different peak intensities – suggesting a fine-grained coesite plus quartz intergrowths (Fig. 2C). The presence of coesite can be also discerned from BSE image contrast, where coesite results with a slightly lighter grey back-scatter signal compared with that of quartz, and this characteristic has been highlighted in Fig. 3 by enhancing contrast.

4.2. Transmission electron microscopy and electron diffraction

Five FIB lamellae were extracted from interface areas between PDF-bearing quartz and coesite and analysed by transmission electron microscopy (TEM) and electron diffraction (ED) (Figs. 4–6, Supplementary material Fig. S6–S8). Each lamella consists of an assemblage of quartz and coesite, in variable ratios. The two phases can be easily distinguished by ED (Fig. 5A), and subordinately by their different contrast in TEM imaging (Fig. 4).

Quartz shows well-developed sets of PDF. At the TEM scale, PDFs are normally slightly open. They may be empty or filled with a low-contrast scoriaceous amorphous material. Where dominant, quartz shows a uniform crystallographic orientation in individual FIB cuts, indicating each lamella and probably the whole particle was a single quartz crystal of the parent rock (Supplementary material Fig. S8).

Coesite ranges in size from ~500 nm to few nanometres, as aggregates of very inhomogeneous crystals. Coesite grains may have rounded or elongated habit and, where suitably oriented, show planar contrast features. 3D ED analysis indicate that such features are the results of twinning and planar disorder along (0 1 0) planes (Fig. 5B, Supplementary material Fig. S7). Coesite grains do not show any evident preferential or reciprocal iso-orientation (Fig. 5A).

Amorphous material was detected only as scoriaceous filling in open PDFs. No appreciable amorphous or 'glassy' volume was detected by TEM inside the FIB lamellae. A diffuse porosity occupies intergranular areas (Fig. 4A). It is not obvious if such porosity is a primary feature of the particle, possibly associated with volume reduction from the transformation of quartz into coesite and subsequent volume expansion during pressure release, or an artefact of sample preparation.

Where quartz and coesite are in contact, quartz boundaries are always lobate or sawtooth-like, with coesite crys-

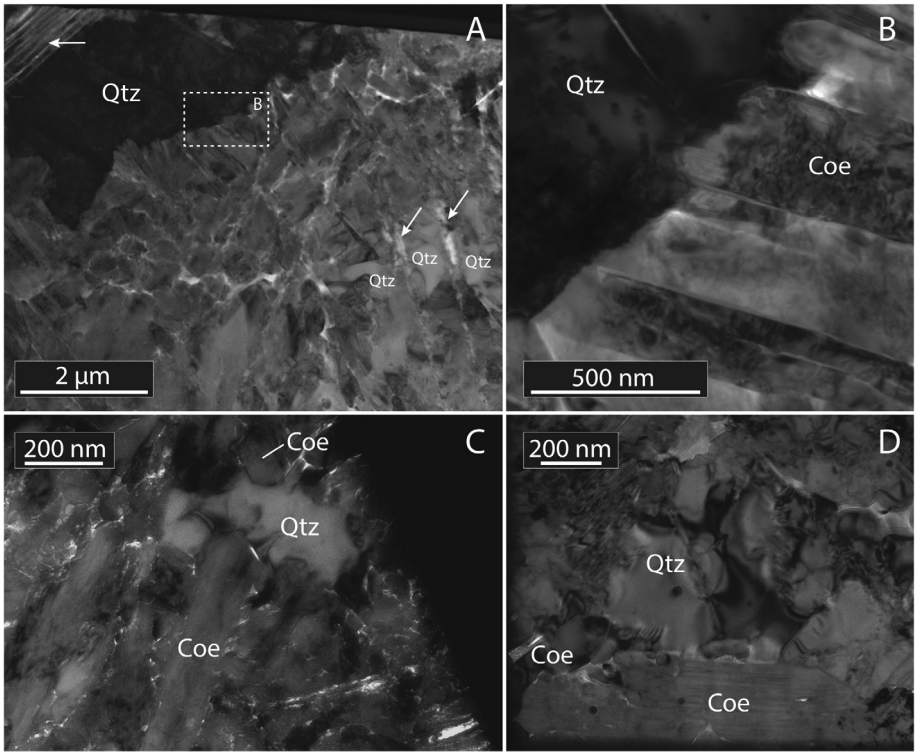

Fig. 4. Bright-field TEM images showing textural relations between coesite (Coe) and PDF-bearing quartz (Qtz). (A) Overview of a FIB lamella showing the textural relationship between quartz and coesite. The arrow in the top-left highlights well-defined PDFs, while the two arrows in the right side of the image highlight possible relict PDFs which extend into the coesite domain. (B) Close-up view of the rectangular area in (A) showing the quartz-coesite contact. Note how coesite crystals grow at the expense of the quartz grain, giving the impression to penetrate inside quartz and forming a characteristic sawtooth-like interface. (C) Relict quartz grain surrounded by several elongated nanometre-scaled coesite grains with an arrowhead shape. (D) ~800 nm long euhedral coesite grain in direct contact with quartz. The PACOM map (EBSD-like) of this image is in Fig. 5.

tals penetrating through the quartz boundaries (Fig. 4B). Coesite crystals show typical euhedral boundaries and arrowhead terminations pointing into quartz crystals (Fig. 4C and D). Coesite and quartz are always in direct contact and no amorphous material was ever observed between. 3D ED and PACOM analysis show a recurrent pseudo iso-orientation between the $\left[1\ \bar{1}\ 1\right]$* quartz areas and [0 1 0]* neighbouring coesite crystals.

Single crystal quartz relicts inside polycrystalline coesite domains often show up to four sets of PDFs. Common PDF orientations are $\{1\ 0\ \bar{1}\ 1\}$ and $\{1\ 0\ \bar{1}\ 2\}$, indicating shock pressure between 20 GPa and 25 GPa on single quartz crystal (Langenhorst and Deutsch, 1994), or ~15 GPa on 25–30 vol.% porous quartzose rocks (Kowitz et al., 2016). Such planar features extend beyond quartz crystal boundaries into the coesite domains over distances of a few tens to several hundreds of nanometres (Fig. 6). Planar features lose coherency in the polycrystalline coesite domains and, when properly oriented, appear to be discontinuous (Supplementary material Fig. S6). Coesite grains on either side of a planar feature differ in orientation.

Despite the finding (using X-ray diffraction) of traces of stishovite in a few shocked-quartz grains from the AAMT layer at Site ODP1144A (Glass and Koeberl, 2006), we found no evidence of this mineral using ED or Raman micro-spectroscopy.

5. DISCUSSION

5.1. Evidence of subsolidus direct quartz-to-coesite transformation

As outlined in the Introduction, it is generally believed that coesite in impact rocks forms by the crystallisation of an amorphous phase. This process would take place during the decompression stage either from silica melt with short-range order and silicon in fourfold coordination (e.g., Stöffler and Langenhorst, 1994), or through a solid-state transformation of diaplectic silica glass (Stähle et al., 2008). Both models are based on direct observations of natural and experimental non-porous rocks and on theoretical considerations: (1) in non-porous rocks, coesite only occurs in association with amorphous silica material (Stöffler, 1971); (2) coesite cannot be produced in shock experiments, possibly due the too short pressure-pulse length reached in laboratory conditions (Stöffler and Langenhorst, 1994); (3) direct quartz-to-coesite transformation is reconstructive

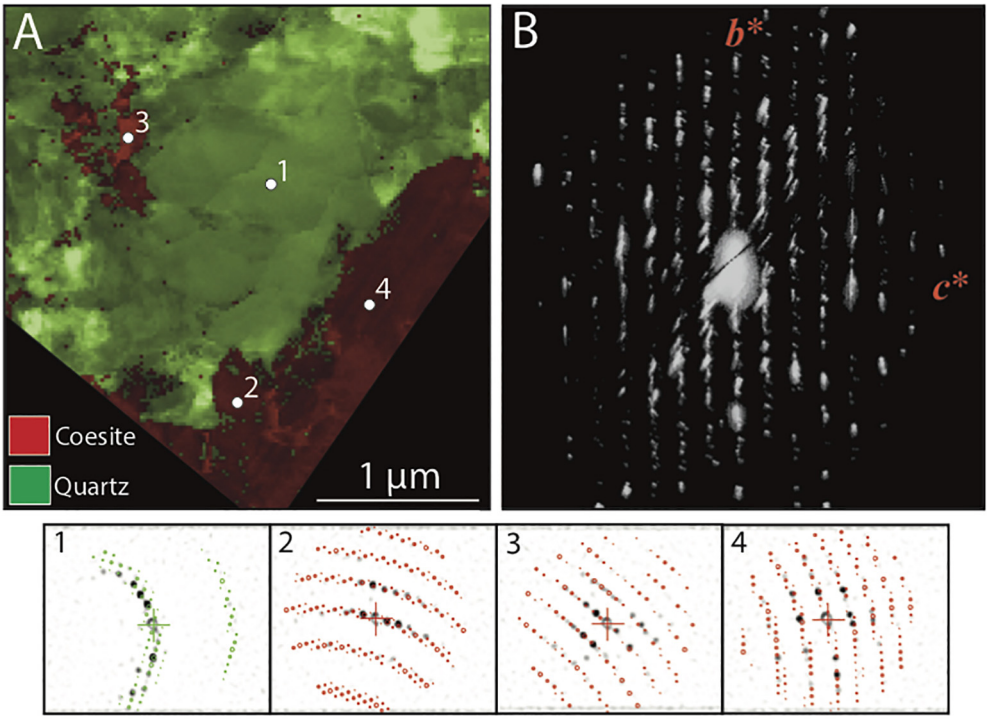

Fig. 5. Electron diffraction data from the silica ejecta particle in Fig. 4D. (A) PACOM map (EBSD-like) of an area in Fig. 4D (rotated ~60° counter-clockwise) showing quartz in green and coesite in red. The four panels labelled 1–4 show electron diffraction data for quartz (1) and coesite (2–4). Quartz has the same orientation throughout the area, suggesting that it has remined as a single quartz grain of the protolith. By contast, coesite grains show patterns with different orientations, suggesting a different nucleation. (B) 3D ED volume of the ~1 µm coesite crystal labelled in (A) with the dot number 4. EDT reveal diffuse scattering along [0 1 0]*, consistent with stacking disorder of (0 1 0) planes. (For interpretation of the references to colour in this figure legend, the reader is referred to the web version of this article.)

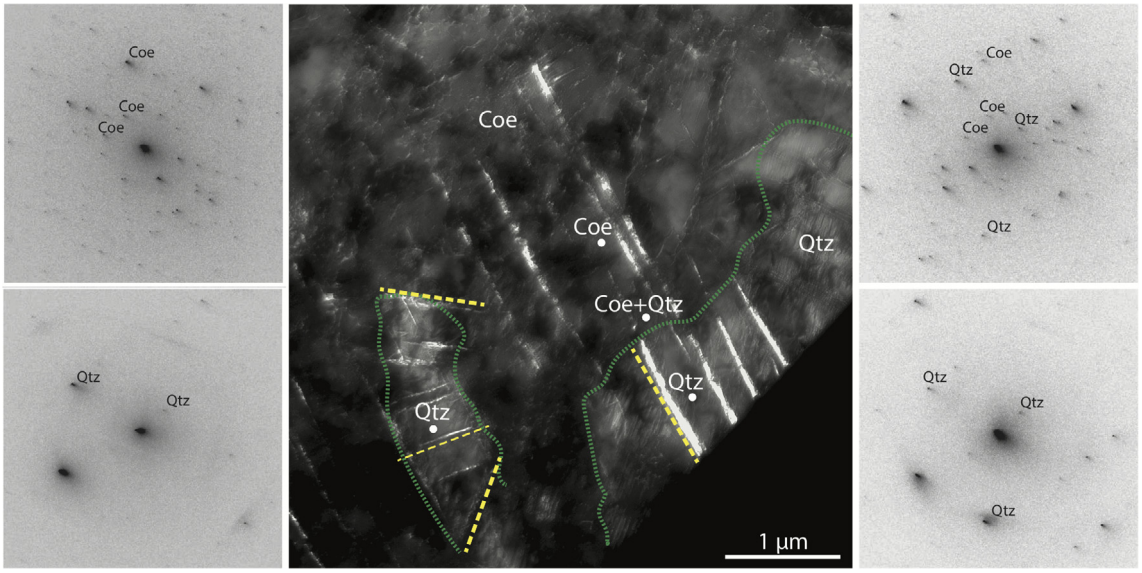

Fig. 6. TEM and ED analysis of the textural relations between polycrystalline coesite (Coe) domains and PDF-bearing quartz (Qtz) areas. Most of the central TEM image is coesite. The edges of two quartz domains are highlighted by a green dotted line. PDF directions are highlighted with yellow dashed lines. PDFs clearly extend from the quartz areas to the coesite domains, where they look irregular, discontinuous, and partially erased. Four diffraction patterns (indicated by white circles) are showen: one of each quartz domain at the bottom, one for coesite (top left), and one showing reflections of both quartz and coesite (top right). (For interpretation of the references to colour in this figure legend, the reader is referred to the web version of this article.)

and hence is presumed to be too time-consuming to take place during compression in impact cratering events, this because the complete collapse of the crystal structure to glass in the solid state is the only possible response to rapid shock compression (e.g. Langenhorst and Deutsch, 2012). On the other hand, the subsolidus direct quartz-to-coesite transformation has recently been proposed for the shocked quartz arenite from the Kamil crater (Egypt) (Folco et al., 2018) to explain the coesite-quartz intergrowths in the so-called symplectic regions. Similar features were first described by Kieffer et al. (1976) in the Coconino sandstone from Barringer crater (Arizona, USA).

The iso-orientation of quartz in the FIB lamellae indicate that the particle '1144A_350' originated as a single quartz grain in the target rock. The direct contact between quartz and microcrystalline coesite and the sawtooth-like geometry of quartz-coesite interface indicate direct quartz-to-coesite transformation (i.e., without the involvement of an intermediate phase) (Fig. 4). Moreover, the euhedral habit of the coesite grains is consistent with a solid-state transformation, with coesite growing at the expense of quartz (Fig. 4). As the polycrystalline coesite domains have sets of planar features that are in textural continuity with PDFs in the adjacent quartz relics, they are interpreted to form at the expense of PDF-bearing quartz (Fig. 6). Thus, coesite must postdate PDF formation in the quartz precursor, and the involvement of a liquid intermediate phase during the quartz-to-coesite transformation can be ruled out (Fig. 6).

We suggest that the subsolidus coesite formation in the studied samples took place through the following temporal sequence: quartz, PDFs, and coesite, with no intermediate amorphous or crystalline phase. The preservation of pristine pressure-induced modifications (i.e. PDFs in quartz, quartz-to-coesite transformation, PDF relicts in polycrystalline coesite domains) and the lack of evidence of thermal annealing suggests rapid cooling, which is consistent with the long-distance transport of the studied ejecta particles. Another possibility to explain the lack of significant amorphous portions is the local attainment of temperatures below the silica liquidus. In fact, the 15–25 GPa indicated by $\{0\ 1\ \bar{1}\ 1\}$ and $\{1\ 0\ \bar{1}\ 2\}$ orientations of PDFs is lower than the 30 GPa critical shock pressure for melting (P_c) of a quartzite rock with 25 vol.% porosity (i.e., the porosity of Coconino sandstone; Wünnemann et al., 2008).

However, it must be noted that the 15–25 GPa required for PDF formation in the studied grain is higher that required for the formation of coesite (3–10 GPa) at equilibrium conditions. In order to reconcile this discrepancy, Folco et al. (2018) suggested that the quartz-to-coesite transformation takes place during decompression and subsequent pressure amplification due to localized shock-wave reverberation connected to the pore collapse process in porous rocks (Güldemeister et al., 2013). Such a mechanism may also be favoured by heterogeneities in the protolith, such as grain boundaries, fractures, inclusions or dislocations, which would also enable the target material to experience high pressure for a longer time. This would provide sufficient time for the subsolidus quartz-to-coesite transformation and could be the dominant mechanism of coesite formation in porous quartz-bearing target rocks, including the postulated parent rocks of the Australasian tektites (e.g., Taylor and Kaye, 1969; Glass and Koeberl, 2006).

It is important to emphasize that during impact cratering events, minerals abruptly adjust to the extreme pressure-temperature conditions imposed by the passage of shock waves at supersonic velocity. Variations in pressure/temperature conditions and phase transitions connected with shock metamorphism occur in timeframes that are orders of magnitude shorter than typical geological processes, and non-equilibrium conditions are the rule rather than the exception. This implies metastability conditions, so that at a given time, P-T coordinates and mineralogical paragenesis may not match in the transition phase diagram. Time (t) plays a pivotal role, and the resulting rock resembles a yield from an incomplete reaction. A short time of reaction, like the one expected for impact metamorphism, results therefore in rocks where phases and shock features like quartz, PDFs, coesite and possibly stishovite can coexist in a non-equilibrium assemblage. This consideration may thus explain why coesite is found in high abundances in rocks that experienced shock pressures far above its equilibrium field.

5.2. Crystallographic relations between quartz and coesite and possible transformation mechanisms

Quartz and coesite grains in direct contact show a recurrent reciprocal orientation, with the $[1\ \bar{1}\ 1]^*$ vector of quartz almost parallel with the $[0\ 1\ 0]^*$ vector of coesite. Indeed, quartz and coesite structures viewed along these directions show striking similarities (Fig. 7A and B). In projection, we can recognise a packing of pseudo-quadratic channels in both mineral structures, whose vertexes consist of columns of Si atoms. When oriented along an orthogonal direction, we observe that such columns are made of 3 and 4 Si atoms for quartz and coesite, respectively (Fig. 7C and D). From this crystallographic perspective it appears that transition from quartz to coesite can be easily accomplished, namely through a martensitic-like transformation consisting of relative structural shifts between $\{\bar{1}\ 0\ 1\ 1\}$ quartz planes and related rearrangement of ionic Si—O—Si bonds to form four Si atoms columns. In this model, quartz $\{\bar{1}\ 0\ 1\ 1\}$ planes turn into coesite $(0\ 1\ 0)$ planes, which are in fact the planes along which disorder and polytypic twinning occur (Fig. 5B, Supplementary material Fig. S7). Note also that $\{1\ 0\ \bar{1}\ 1\}$ is one of the most recurrent PDF families in shocked quartz-bearing rocks, including the AAMT layer ejecta particle studied in this work. From a structural point of view $\{\bar{1}\ 0\ 1\ 1\}$ and $\{1\ 0\ \bar{1}\ 1\}$ planes are not equivalent in the trigonal system (to which alpha-quartz belongs): however, these planes cannot be distinguished by geometry.

Nonetheless, due to the rapid shock compression the only possible phase transition of quartz is the collapse of the crystal lattice to glass in the solid state, i.e. diaplectic glass at 30–35 GPa (e.g. Langenhorst and Deutsch, 2012). Based on these statements, it would appear that because

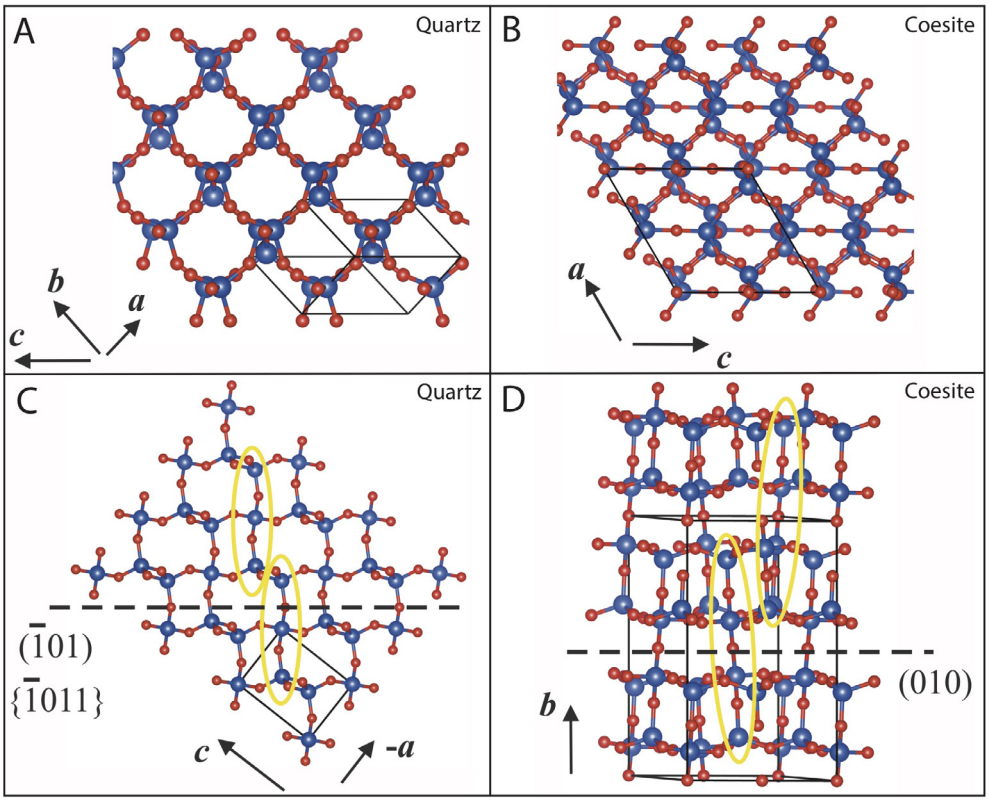

Fig. 7. Comparison between quartz and coesite crystal structures. (A) Quartz structure viewed along [1 $\bar{1}$ 1], which is ~6° from [1 $\bar{1}$ 1]*. (B) Coesite structure viewed along [0 1 0]. (C) Quartz structure viewed along [0 1 0]. Two 3-Si columns are highlighted in yellow and the (1 0 1) plane, belonging to the {1 0 1 1} family, is marked by a black dashed line. (D) Coesite structure viewed along a direction almost orthogonal to [0 1 0]. Two 4-Si columns are highlighted in yellow and the (0 1 0) plane is marked by a black dashed line. Cell parameters are sketched in black, Si atoms in blue, O atoms in red. (For interpretation of the references to colour in this figure legend, the reader is referred to the web version of this article.)

the quartz-to-coesite transformation is reconstructive, it is presumably too time-consuming to take place during the compression stage during impact cratering events. However, there are many examples of subsolidus polymorphic transition in impact cratering events, despite their reconstructive nature. These processes usually occur via diffusionless mechanisms. Probably, the best-known example is the graphite-to-diamond transformation (Masaitis et al., 1972). Other common solid-state polymorphic transitions include reidite (high-pressure polymorph of zircon with scheelite-type structure; Glass et al., 2002) and two different high-pressure polymorphs of rutile, namely TiO_2-II and akaogiite (with columbite- and baddeleyite-type structures, respectively; El Goresy et al., 2001, 2010). Some of these generally acknowledged phase transitions induced by shock metamorphism are structurally more striking than quartz-to-coesite transformation. For example, in graphite-to-diamond and in rutile-to-akaogiite transformations C and Ti change their atomic coordination state, from 3 to 4 and from 6 to 7, respectively. All these phase transitions are diffusionless-type transformations – to which twinning also belongs – in which the crystal structure is distorted through a cooperative movement of atoms or through shear (martensitic-type), without long-range diffusion (Fultz, 2014).

Quartz and coesite structures are both based on a network of SiO_4 tetrahedra, where silicon is similarly coordinated with 4 oxygen atoms. The actual mechanism that allows the transformation from one structure to the other is not evident because there are many possible rearrangements that may lead quartz network to coesite. Moreover, a very fast change in PT conditions, like the one triggered by impact events, may allow phase transitions pathways different from those inferred from results of static anvil-cell experiments (Bourova et al., 2004; Durandurdu, 2009; Merli and Sciascia, 2013). Finally, the pervasive planar disorder and polysynthetic nano-twinning typical of impact-coesite may play a role in accelerating the rate of coesite formation and reducing the activation energy required.

The model described here explains the formation of coesite at lower shock pressures and over shorter durations typical of shock wave propagation scenarios, thus accounting for its presence in materials that did not experienced melting – which require shock pressure higher than 30 GPa for porous rocks. A decrease of peak pressure required for the coesite formation provides fundamental constraints on the physical condition attained during impacts in quartz-bearing porous target rocks, and a re-evaluation (i.e., reduction) of peak shock pressure estimates may be necessary.

6. CONCLUSIONS

This work provides electron diffraction evidence for the direct subsolidus quartz-to-coesite transformation in shocked coesite-bearing quartz ejecta from the Australasian tektite/microtektite strewn field. This transformation postdates PDF formation in the quartz precursor. This is in contrast with previous studies, mostly based on observations from crystalline rocks, which suggested that impact-formed coesite is the product of rapid crystallization from silica melt or diaplectic glass during shock unloading, when the pressure release path passes through the coesite stability field (e.g., Stöffler and Langenhorst, 1994; Stähle et al., 2008).

We explain the subsolidus quartz-to-coesite transformation through a martensitic-like process, in which a relative structural shift of $\{\bar{1}\ 0\ 1\ 1\}$ quartz planes turn them into coesite (0 1 0) planes. This mechanism would also correlate the diagnostic disorder and twinning of impact coesite along (0 1 0) composition planes with the $\{1\ 0\ \bar{1}\ 1\}$ PDF family commonly observed in quartz. Arguably, the subsolidus quartz-to-coesite transformation through a martensitic-like process could be the dominant mechanism of coesite formation in a wide range of cratering events, at least in those where porous target rocks were involved, like at the Barringer (Kieffer et al., 1976) and Kamil craters (Folco et al., 2018).

The quartz-to-coesite transformation model proposed here is based on the ED study of a few samples only. A future detailed ED investigation of both crystalline and porous target rocks from different impact structures may provide additional insight into quartz-coesite relations and phase transition phase paths, helping to understand whether the direct subsolidus quartz-to-coesite transformation is specific for porous target rocks or whether is the norm in impact events regardless of the target type (porous or crystalline).

The preservation of the fine quartz-coesite textural and microstructural relationships, such as those observed in this work, depend on the extent of the post-shock thermal overprint commonly observed in shock metamorphic rocks (e.g., Fazio et al. 2017). Pristine features, such as those found in the ejecta particles from the Australasian microtektite layer studied here, represent an excellent opportunity to investigate the mechanism and kinetics of the direct subsolidus quartz-to-coesite transformation during shock metamorphic events.

This work shows the potential of the emerging 3D ED method for the structure characterization of materials available only as sub-micrometer-sized grains (Gemmi et al., 2019), thereby opening a new perspective in shock metamorphic studies, given the micro-to-nanometer scale of shock metamorphic features and their defective nature. Interestingly, by using very mild illumination conditions, complete and high-resolution data can be collected on phases that normally deteriorate rapidly in high resolution TEM mode (such as high pressure SiO_2 phases and nucleation seeds in amorphous areas). Likewise, the PACOM technique enables reliable phase/orientation maps (EBSD/TKD-like) with a spatial resolution down to 2 nm when used with a field emission gun, which is well below the 20–50 nm achieved with EBSD and similar to the spatial resolution achieved by TKD (Sneddon et al., 2016). Also, whilst yielding less precise orientation measurements when compared with Kikuchi lines in EBSD, spot diffraction patterns are less affected by the distortion induced by high dislocation densities (Viladot et al., 2013). Therefore, PACOM is particularly suited for investigating strongly plastically deformed materials like the shocked silica ejecta studied here.

ACKNOWLEDGEMENTS

We would like to thank Billy Smith and Colin How (University of Glasgow) for their technical assistance with the FIB and the TEM and Randa Ishak (CISIM, Università di Pisa) for her support during SEM data acquisition. We also thank Catherine A. Macris, one anonymous reviewer and Associate Editor Christian Koeberl for their suggestions and constructive comments during the review process. This work was supported by MIUR-Programma Nazionale delle Ricerche in Antartide (ID# PNRA16_00029/ P.I. LF) and by the UK Science and Technology Facilities Council through grant ST/N000846/1. This study is part of Fabrizio Campanale's PhD thesis of the Corso di Dottorato Regionale 2018/2019, XXXIV ciclo, which is funded by the Istituto Italiano di Tecnologia (IIT).

APPENDIX A. SUPPLEMENTARY MATERIAL

Supplementary data to this article can be found online at https://doi.org/10.1016/j.gca.2019.08.014.

REFERENCES

Amare K. and Koeberl C. (2006) Variation of chemical composition in Australasian tektites from different localities in Vietnam. *Meteorit. Planet. Sci.* **123**, 107–123. https://doi.org/10.1111/j.1945-5100.2006.tb00196.x.

Bourova E., Parker S. C. and Richet P. (2004) High-temperature structure and dynamics of coesite (SiO_2) from numerical simulations. *Phys. Chem. Miner.* **31**, 569–579. https://doi.org/10.1007/s00269-004-0395-x.

Bourret A., Hinze E. and Hochheimer H. D. (1986) Twin structure in coesite studied by high resolution electron microscopy. *Phys. Chem. Miner.* **13**, 206–212. https://doi.org/10.1007/BF00308163.

Chao E. C. T., Shoemaker E. M. and Madsen B. M. (1960) First natural occurrence of coesite. *Science* **132**, 220–222. https://doi.org/10.1126/science.132.3421.220.

Coes L. (1953) A new dense crystalline silica. *Science* **118**, 131–132. https://doi.org/10.1126/science.118.3057.131.

De Wolf I. (1996) Micro-Raman spectroscopy to study local mechanical stress in silicon integrated circuits. *Semicond. Sci. Technol.* **11**, 139–154. https://doi.org/10.1088/0268-1242/11/2/001.

Durandurdu M. (2009) Formation of an anataselike phase in silica under anisotropic stress: an ab initio constant-pressure study. *Phys. Rev. B* **80**, 1–5. https://doi.org/10.1103/PhysRevB.80.024102.

El Goresy A., Chen M., Gillet P., Dubrovinsky L., Graup G. and Ahuja R. (2001) A natural shock-induced dense polymorph of rutile with α-PbO_2 structure in the suevite from the Ries Crater

in Germany. *Earth Planet. Sci. Lett.* **192**, 485–495. https://doi.org/10.1016/s0012-821x(01)00480-0.

El Goresy A., Dubrovinsky L., Gillet P., Graup G. and Chen M. (2010) Akaogiite: An ultra-dense polymorph of TiO_2 with the baddeleyite-type structure, in shocked garnet gneiss from the Ries Crater, Germany. *Am. Mineral.* **95**, 892–895. https://doi.org/10.2138/am.2010.3425.

Fazio A., Folco L., D'Orazio M., Frezzotti M. L. and Cordier C. (2014) Shock metamorphism and impact melting in small impact craters on Earth: evidence from Kamil Crater, Egypt. *Meteorit. Planet. Sci.* **49**, 1–26. https://doi.org/10.1111/maps.12385.

Fazio A., Mansfeld U. and Langenhorst F. (2017) Coesite in suevite from the Ries impact structure (Germany): from formation to postshock evolution. *Meteorit. Planet. Sci.* **52**, 1437–1448. https://doi.org/10.1111/maps.12849.

Folco L., Rochette P., Perchiazzi N., D'Orazio M., Laurenzi M. A. and Tiepolo M. (2008) Microtektites from Victoria land transantarctic mountains. *Geology* **36**, 291–294. https://doi.org/10.1130/G24528A.1.

Folco L., Glass B. P., D'Orazio M. and Rochette P. (2010) A common volatilization trend in Transantarctic Mountain and Australasian microtektites: implications for their formation model and parent crater location. *Earth Planet. Sci. Lett.* **293**, 135–139. https://doi.org/10.1016/j.epsl.2010.02.037.

Folco L., D'Orazio M., Gemelli M. and Rochette P. (2016) Stretching out the Australasian microtektite strewn field in Victoria Land Transantarctic Mountains. *Polar Sci.* **10**, 147–159. https://doi.org/10.1016/j.polar.2016.02.004.

Folco L., Mugnaioli E., Gemelli M., Masotta M. and Campanale F. (2018) Direct quartz-coesite transformation in shocked porous sandstone from Kamil Crater (Egypt). *Geology* **46**, 739–742.

Fultz B. (2014) Diffusionless transformations. In *Phase Transitions in Materials*. Cambridge University Press, Cambridge, pp. 355–382. https://doi.org/10.1017/CBO9781107589865.019.

Gemmi M., Mugnaioli E., Gorelik T. E., Kolb U., Palatinus L., Boullay P., Hovmöller S. and Abrahams J. P. (2019) 3D electron diffraction: the nanocrystallography revolution. *ACS Cent. Sci.*. https://doi.org/10.1021/acscentsci.9b00394.

Glass B. P. and Barlow R. A. (1979) Mineral inclusions in Muong Nong-type indochinites – implications concerning parent material and process of formation. *Meteoritics* **14**, 55–67. https://doi.org/10.1111/j.1945-5100.1979.tb00479.x.

Glass B. P. and Fries M. (2008) Micro-Raman spectroscopic study of fine-grained, shock-metamorphosed rock fragments from the Australasian microtektite layer. *Meteorit. Planet. Sci.* **43**, 1487–1496. https://doi.org/10.1111/j.1945-5100.2008.tb01023.x.

Glass B. P. and Koeberl C. (2006) Australasian microtektites and associated impact ejecta in the South China Sea and the Middle Pleistocene supereruption of Toba. *Meteorit. Planet. Sci.* **41**, 305–326. https://doi.org/10.1111/j.1945-5100.2006.tb00211.x.

Glass B. P. and Simonson B. M. (2013) *Distal Impact Ejecta Layers: A Record of Large Impacts in Sedimentary Deposits*. Springer, Heidelberg, New York, Dordrecht, London.

Glass B. P. and Wu J. (1993) Coesite and shocked quartz discovered in the Australasian and North American microtektite layers. *Geology* **21**, 435–438. https://doi.org/10.1130/0091-7613(1993) 021<0435:CASQDI>2.3.CO;2.

Glass B. P., Liu S. and Leavens P. B. (2002) Reidite: an impact-produced high-pressure polymorph of zircon found in marine sediments. *Am. Mineral.* **87**, 562–565. https://doi.org/10.2138/am-2002-0420.

Grady D. E., Murri W. J. and De Carli P. S. (1975) Hugoniot sound velocities and phase transformations in two silicates. *J. Geophys. Res.* **80**, 4857–4861. https://doi.org/10.1029/JB080i035p04857.

Güldemeister N., Wünnemann K., Durr N. and Hiermaier S. (2013) Propagation of impact-induced shock waves in porous sandstone using mesoscale modeling. *Meteorit. Planet. Sci.* **48**, 115–133. https://doi.org/10.1111/j.1945-5100.2012.01430.x.

Kieffer S. W., Phakey P. P. and Christie J. M. (1976) Shock processes in porous quartzite: transmission electron microscope observations and theory. *Contrib. Mineral. Petrol.* **59**, 41–93. https://doi.org/10.1007/BF00375110.

Koeberl C. (1992) Geochemistry and origin of Muong Nong-type tektites. *Geochim. Cosmochim. Acta* **56**, 1033–1064. https://doi.org/10.1016/0016-7037(92)90046-L.

Koeberl C. (1994) Tektite origin by hypervelocity asteroidal or cometary impact: Target rocks, source craters, and mechanisms. In *Large Meteorite Impacts and Planetary Evolution. GSA Special Paper*, 293 (eds. B. O. Dressler, R. A. F. Grieve and V. L. Sharpton), pp. 133–152. https://doi.org/10.1130/SPE293-p133.

Kolb U., Mugnaioli E. and Gorelik T. E. (2011) Automated electron diffraction tomography – a new tool for nano crystal structure analysis. *Cryst. Res. Technol.* **46**, 542–554. https://doi.org/10.1002/crat.201100036.

Kowitz A., Uldemeister N. G., Schmitt R. T., Reimold W., Holzwarth A. and Unnemann K. W. (2016) Revision and recalibration of existing shock classifications for quartzose rocks using low-shock pressure (2.5 – 20 GPa) recovery experiments and mesoscale numerical modeling. *Meteorit. Planet. Sci.* **51**, 1741–1761. https://doi.org/10.1111/maps.12712.

Langenhorst F. and Deutsch A. (1994) Shock experiments on pre-heated α- and β-quartz: I. Optical and density data. *Earth Planet. Sci. Lett.* **128**, 407–420. https://doi.org/10.1016/0012-821X(94)90229-1.

Langenhorst F. and Deutsch A. (2012) Shock metamorphism of minerals. *Elements* **8**, 31–36. https://doi.org/10.2113/gselements.8.1.31.

Lee M., Bland P. A. and Graham G. (2003) Preparation of TEM samples by focused ion beam (FIB) techniques: applications to the study of clays and phyllosilicates in meteorites. *Mineral. Mag.* **67**, 581–592. https://doi.org/10.1180/0026461036730119.

Liu L., Mernagh T. and Hibberson W. O. (1997) Raman spectra of high-pressure polymorphs of SiO_2 at various temperatures. *Phys. Chem. Miner.* **24**, 396–402. https://doi.org/10.1007/s002690050053.

Luo S. N., Ahrens T. J. and Asimow P. D. (2003) Polymorphism, superheating, and amorphization of silica upon shock wave loading and release. *J. Geophys. Res. B* **108**, 1–13. https://doi.org/10.1029/2002JB002317.

Ma P., Aggrey K., Tonzola C., Schnabel C., De Nicola P., Herzog G. F., Wasson J. T., Glass B. P., Brown L., Tera F., Middleton R. and Klein J. (2004) Beryllium-10 in Australasian tektites: constraints on the location of the source crater. *Geochim. Cosmochim. Acta* **68**, 3883–3896. https://doi.org/10.1016/j.gca.2004.03.026.

Martini J. E. J. (1978) Coesite and stishovite in the Vredefort Dome, South Africa. *Nature* **272**, 715–717. https://doi.org/10.1038/272715a0.

Martini J. E. J. (1991) The nature, distribution and genesis of the coesite and stishovite associated with the pseudotachylite of the Vredefort Dome, South Africa. *Earth Planet. Sci. Lett.* **103**, 285–300. https://doi.org/10.1016/0012-821X(91)90167-G.

Masaitis V. L., Futergendler S. I. and Gnevushev M. A. (1972) Diamonds in impactites of the Popigai meteorite crater (in Russian). *Proc. All-Union Mineral. Soc.* **1**, 108–112.

Melosh H. J. (2012) The contact and compression stage of impact cratering. In *Impact Cratering* (eds. G. R. Osinski and E. Pierazzo). Blackwell Publishing Ltd, Chichester. https://doi.org/10.1002/9781118447307.ch3.

Merli M. and Sciascia L. (2013) Bader's topological analysis of the electron density in the pressure-induced phase transitions/amorphization in α-quartz from the catastrophe theory viewpoint. *Phys. Chem. Miner.* **40**, 455–466. https://doi.org/10.1007/s00269-013-0583-7.

Mizera J., Řanda Z. and Kameník J. (2016) On a possible parent crater for Australasian tektites: Geochemical, isotopic, geographical and other constraints. *Earth-Sci. Rev.* **154**, 123–137. https://doi.org/10.1016/j.earscirev.2015.12.004.

Mugnaioli E. and Gemmi M. (2018) Single-crystal analysis of nanodomains by electron diffraction tomography: mineralogy at the order-disorder borderline. *Z. Kristallogr. Cryst. Mater.* **233**, 1–16. https://doi.org/10.1515/zkri-2017-2130.

Nederlof I., van Genderen E., Li Y. W. and Abrahams J. P. (2013) A Medipix quantum area detector allows rotation electron diffraction data collection from submicrometre three-dimensional protein crystals. *Acta Crystallogr. D* **69**, 1223–1230. https://doi.org/10.1107/S0907444913009700.

Rochette P., Braucher R., Folco L., Horng C. S., Aumaître G., Bourlès D. L. and Keddadouche K. (2018) ^{10}Be in Australasian microtektites compared to tektites: Size and geographic controls. *Geology* **46**, 803–806. https://doi.org/10.1130/G45038.1.

Scott J. F. and Porto S. P. S. (1967) Longitudinal and transverse optical lattice vibrations in quartz. *Phys. Rev.* **161**, 903–910. https://doi.org/10.1103/PhysRev.161.903.

Shoemaker E. M. and Chao E. C. T. (1961) New evidence for the impact origin of the Ries Basin, Bavaria, Germany. *J. Geophys. Res.* **66**, 3371–3378. https://doi.org/10.1029/JZ066i010p03371.

Smyth J. R. and Hatton C. J. (1977) A coesite-sanidine grospydite from the Roberts Victor kimberlite. *Earth Planet. Sci. Lett.* **34**, 284–290. https://doi.org/10.1016/0012-821X(77)90012-7.

Sneddon G., Trimby P. and Cairney J. (2016) Transmission Kikuchi diffraction in a scanning electron microscope: a review. *Mater. Sci. Eng. R Rep.* **110**, 1–12. https://doi.org/10.1016/j.mser.2016.10.001.

Spray J. G. and Boonsue S. (2018) Quartz–coesite–stishovite relations in shocked metaquartzites from the Vredefort impact structure, South Africa. *Meteorit. Planet. Sci.* **53**, 93–109. https://doi.org/10.1111/maps.12997.

Stähle V., Altherr R., Koch M. and Nasdala L. (2008) Shock-induced growth and metastability of stishovite and coesite in lithic clasts from suevite of the Ries impact crater (Germany). *Contrib. Mineral. Petrol.* **155**, 457–472. https://doi.org/10.1007/s00410-007-0252-2.

Stöffler D. (1971) Coesite and stishovite in shocked crystalline rocks. *J. Geophys. Res. D* **76**, 5474–5488. https://doi.org/10.1029/JB076i023p05474.

Stöffler D. and Langenhorst F. (1994) Shock Metamorphism of quartz in nature and experiment: I. Basic observation and theory. *Meteoritics* **29**, 155–181. https://doi.org/10.1111/j.1945-5100.1994.tb00670.x.

Taylor S. R. (1962) Fusion of soil during meteorite impact, and the chemical composition of tektites. *Nature* **195**, 32–33. https://doi.org/10.1038/195032a0.

Taylor S. R. (1973) Tektites: a post-Apollo view. *Earth-Sci. Rev.* **9**, 101–123. https://doi.org/10.1016/0012-8252(73)90074-3.

Taylor S. R. and Kaye M. (1969) Genetic significance of the chemical composition of tektites: s review. *Geochim. Cosmochim. Acta* **33**, 1083–1100. https://doi.org/10.1016/0016-7037(69)90064-7.

Viladot D., Véron M., Gemmi M., Peiró F., Portillo J., Estradé S., Mendoza J., Llorca-Isern N. and Nicolopoulos S. (2013) Orientation and phase mapping in the transmission electron microscope using precession-assisted diffraction spot recognition: state-of-the-art results. *J. Microsc.* **252**, 23–34. https://doi.org/10.1111/jmi.12065.

Wackerle J. (1962) Shock-wave compression of quartz. *J. Appl. Phys.* **33**, 922–937. https://doi.org/10.1063/1.1777192.

Wasson J. T. (2003) Large aerial bursts: an important class of terrestrial accretionary events. *Astrobiology* **3**, 163–179. https://doi.org/10.1089/153110703321632499.

Wünnemann K., Collins G. S. and Osinski G. R. (2008) Numerical modelling of impact melt production in porous rocks. *Earth Planet. Sci. Lett.* **269**, 530–539. https://doi.org/10.1016/j.epsl.2008.03.007.

Associate editor: Christian Koeberl